**Electronic Supporting Information**

# Scalable and green juglone synthesis using heterogeneous photocatalysis in a photomicroreactor

Mohsin Pasha,[a] Yuhan Wang,[a] You Ma, [a] Guozhi Qian,[a] Xiao Xue,[a] Hong Zhang,[b] Yong Yang,[c] Minjing Shang,*[a] Pengfei Zhang [d] and Yuanhai Su*[a,d]

| | |
|---|---|
| [a] | Mohsin Pasha, Yuhan Wang, You Ma, Guozhi Qian, Xiao Xue, Minjing Shang, Prof. Yuanhai Su* |
| | School of Chemistry and Chemical Engineering, |
| | Key Laboratory of Thin Film and Microfabrication (Ministry of Education), |
| | Shanghai Jiao Tong University, Shanghai, 200240, PR China |
| [b] | Hong Zhang |
| | School of Chemistry and Chemical Engineering, |
| | Harbin Institute of Technology, |
| | Harbin, Heilongjiang 150001, PR China |
| [c] | Yong Yang |
| | National & Local Joint Engineering Research Center for Mineral Salt Deep Utilization |
| | Faculty of Chemical Engineering, Huaiyin Institute of Technology, |
| | Huaian 223003, PR China |
| [d] | Prof. Pengfei Zhang, Prof. Yuanhai Su* |
| | College of Material, Chemistry and Chemical Engineering, |
| | Hangzhou Normal University, |
| | Hangzhou 311121, China |

Email: mshang@sjtu.edu.cn; y.su@sjtu.edu.cn

## Material and Reagents

Chemicals including napthalene-1,5-diol (DHN, purity 99.01%) and juglone (purity ≥ 97.0%) were respectively bought from Shanghai Beide Pharmaceutical Technology Co., Ltd. and Shanghai Aladdin Bio-Chem Technology Co., Ltd. Photosensitizers containing meso-tetra(4-carboxyphenyl)porphine (m-TcPP, purity ≥ 98.0%) and 5,10,15,20-Tetrakis(1-methyl-4-pyridinio)porphyrin tetra(p-toluenesulfonate) (TMPyP, purity ≥ 97.0%) were purchased from Shanghai Titan Scientific Co. Ltd and Shanghai Gaoxin Chemical Glass Instrument Co., Ltd., respectively. Ion-exchange resin Amberlyst®15 and silicone 60 (230-400 mesh) were employed as catalyst support or base and supplied by Shanghai Gaoxin Chemical Glass Instrument Co., Ltd and Shanghai Titan Technology Co., Ltd., respectively. Furthermore, isopropanol (i-PrOH, AR>99.5%), acetonitrile (MeCN, AR=99.0%), methanol (MeOH, AR=99.0%) and tetrahydrofuran (THF, AR=

99.0%) were purchased from Meryer (Shanghai) Biochemical Technology Co., Ltd, while ethanol (EtOH, AR > 99.0%), hexane (Hx, AR=97.0%), ethyl acetate (EtOAc, AR >99.5%) were purchased from Shanghai Titan Scientific Co., Ltd. Oxygen with a purity ≥ 99.5% (v/v) was supplied by Air liquid Co., Limited (Shanghai, China). All reagents were directly used for the experiments without further purification.

**SEM and EDS characterizations details**
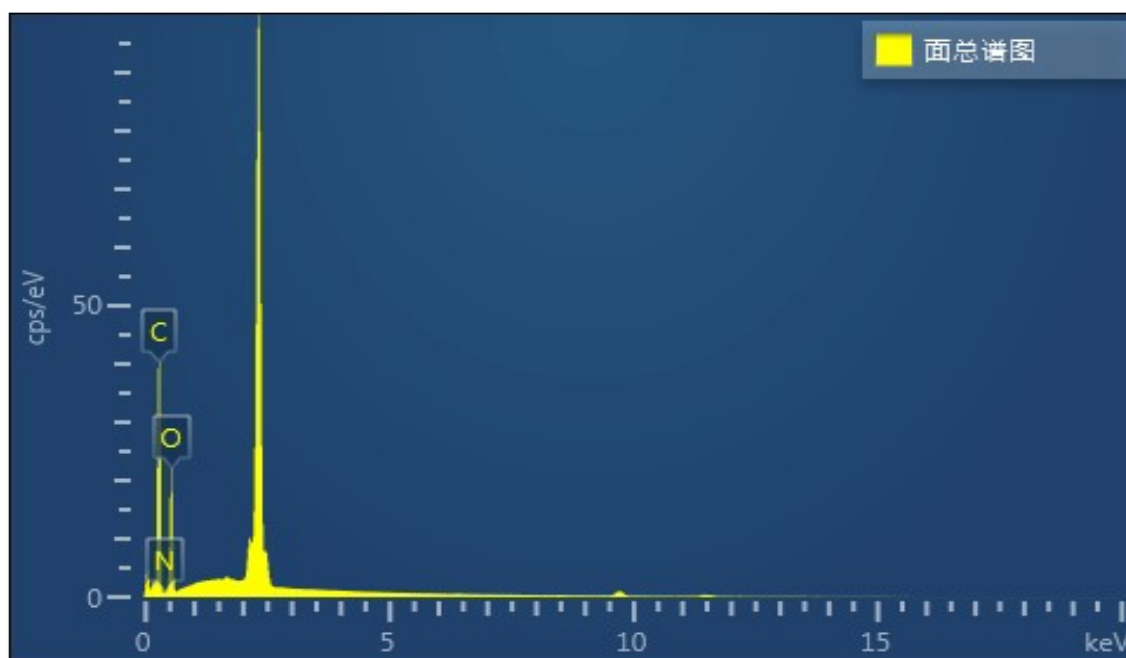


| Element | Line Type | App. Conc. | K ratio | Wt.% | Wt.% Sigma | Atomic % | Std. Sample label | Manufacturer Std. |
|---------|-----------|------------|---------|------|------------|----------|-------------------|-------------------|
| C | K Line system | 10.09 | 0.10095 | 57.09 | 0.13 | 63.93 | C Vit | Yes |
| N | K Line System | 0.00 | 0.00000 | 0.00 | 0.45 | 0.00 | BN | Yes |
| O | K Line System | 8.20 | 0.02759 | 42.91 | 0.13 | 36.07 | SiO2 | Yes |
| Total: | | | | 100.00 | | 100. 00 | | |

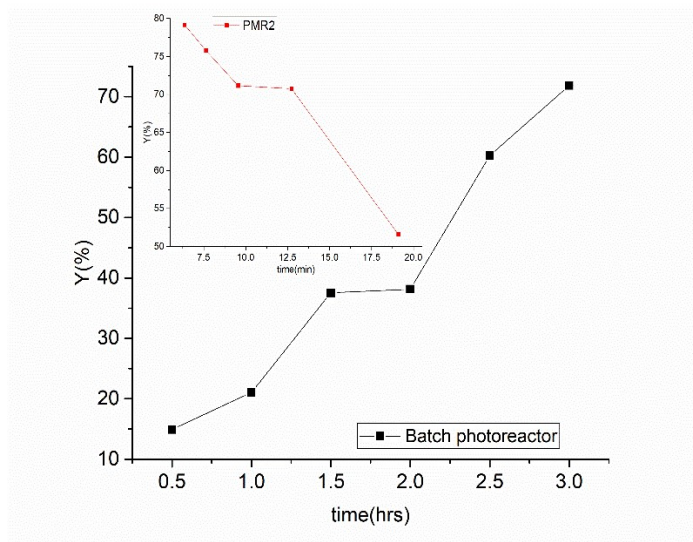**Heterogeneous DHN photooxidation in batch photoreactor and PMR2**



**Fig.S1** Comparison of batch photoreactor with PMR2

Conditions in PMR2: $Q_L$=0.5-1.5 ml/min, $Q_G$=30-60 ml/min, $\tau_{PMR2}$=6.36-19.1 min, Amb-m-TcPP, solvent=i-PrOH, P=360 W and $C_{DHN}$ =0.05 M

Conditions in batch photoreactor: DHN solution volume= 50 ml, $Q_G$=30 ml/min, Amb-m-TcPP weight=3.6 g, $P$=75 W, $C_{DHN}$ =0.01 M and solvent=$i$-PrOH

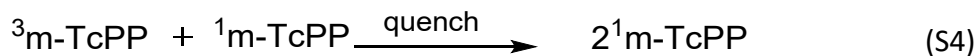**SEM and EDS images of regenerated Amb-m-TcPP (Amb-m-TcPP(R))**
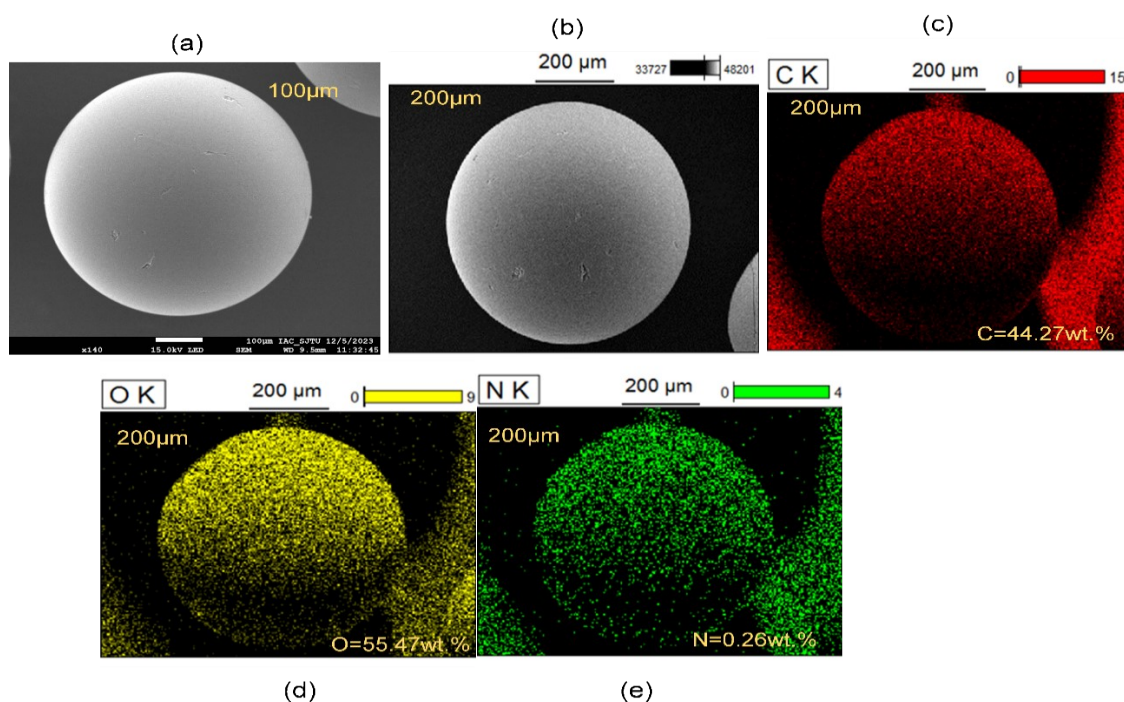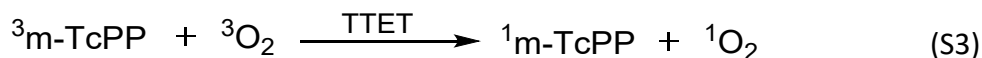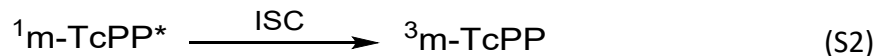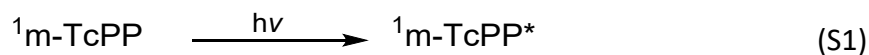
**Amb-m-TcPP leaching potential and stability analysis**
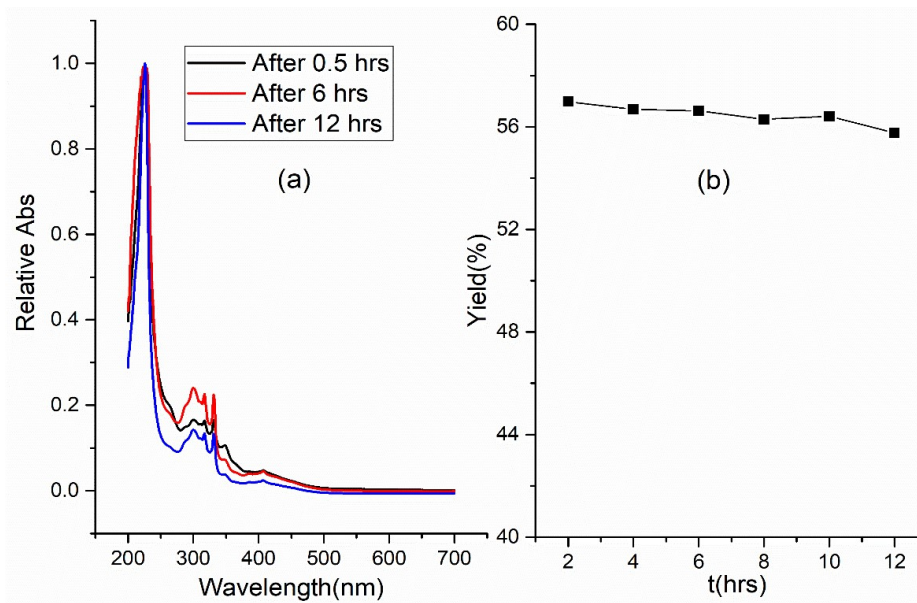


Details for both analysis: (a) UV-Vis absorption spectra of the reaction solution at three different reaction time (b) Amb-m-TcPP stability examination for 12 hours DHN photooxidation campaign, Reaction conditions: Amb-m-TcPP, QL=0.5 ml/min, QG=30 ml/min, CDHN = 0.025M, P=360W, and the solvent was i-PrOH.

**Kinetic modelling of DHN photooxidation and juglone formation steps**

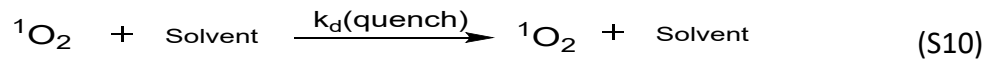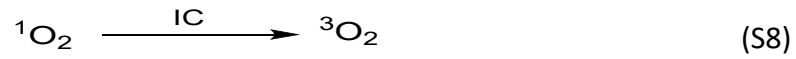The kinetics steps involved in the DHN photooxidation using singlet oxygens are as follows;

$$^1\text{m-TcPP} \xrightarrow{\ h\nu\ } \ ^1\text{m-TcPP*} \tag{S1}$$

$$^1\text{m-TcPP*} \xrightarrow{\ \text{ISC}\ } \ ^3\text{m-TcPP} \tag{S2}$$

$$^3\text{m-TcPP} + \ ^3\text{O}_2 \xrightarrow{\ \text{TTET}\ } \ ^1\text{m-TcPP} + \ ^1\text{O}_2 \tag{S3}$$

$$^3\text{m-TcPP} + \ ^1\text{m-TcPP} \xrightarrow{\ \text{quench}\ } 2\,^1\text{m-TcPP} \tag{S4}$$

$$\text{DHN} + \ ^1\text{O}_2 \xrightarrow{\ k_{obs}\ } \text{Juglone} + \text{H}_2\text{O} \tag{S5}$$

where $^1$m-TcPP, $^1$m-TcPP$^*$ and $^3$m-TcPP mean m-TcPP with ground state, excited state and triplet state, respectively. $^3$O$_2$ and $^1$O$_2$ indicate singlet and triplet oxygen, while ISC, TTET and quench represent intersystem crossing, triplet-triplet energy transfer and quenching processes, respectively. The kinetic model for DHN photooxidation (DHN consumption) and juglone formation steps are as given below:

$$\frac{dC_{DHN}}{dt} = -k_{obs}C_{DHN}C_{^1O_2} \tag{S6}$$

$$\frac{dC_{Juglone}}{dt} = k_{obs}C_{DHN}C_{^1O_2} \tag{S7}$$

In order to express singlet oxygen concentration in terms of rate constants of intermediate steps, we need to incorporate deactivation and quenching of singlet oxygen using internal conversion, fluorescence and solvent, which can be expressed through the subsequent

$$^1O_2 \xrightarrow{\text{IC}} {}^3O_2 \tag{S8}$$

$$^1O_2 \xrightarrow{\text{FL}} {}^3O_2 + h\nu \text{ UV-Vis} \tag{S9}$$

$$^1O_2 + \text{Solvent} \xrightarrow{k_d(\text{quench})} {}^1O_2 + \text{Solvent} \tag{S10}$$

steps.

where IC, FL and $k_d$(quench) indicate internal conversion, fluorescence and physical rate constant through solvent quenching. Mass balance on singlet oxygen leads to the subsequent kinetic model.

$$\frac{dC_{^1O_2}}{dt} = -k_{IC}C_{^1O_2} - k_{FL}C_{^1O_2} - k_dC_{^1O_2}C_{solvent} + k_{TTET}C_{^3m-TcPP}C_{^3O_2} - k_{obs}C_{DHN}C_{^1O_2} \tag{S11}$$

Murata et al.[1] highlighted that the concentration of 1O2 remained constant during the initial reaction stage, and it was supported by the fact that the initial concentration of 3O2 was

much higher compared to DHN and m-TcPP. Based on this evidence and former kinetic investigations on the DHN photooxidation in batch photoreactors[1, 2], the overall reaction rate was mainly determined from the DHN concentration. Thus, the rate of change of singlet oxygen can be considered as zero. Simplification of Equation S11 leads to the following equation.

$$C_{^1O_2} = \frac{k_{TTET}C_{^3m-TcPP}C_{^3O_2}}{k_{IC} + k_{FL} + k_d C_{solvent} + k_{obs}C_{DHN}} \tag{S12}$$

Use this Equation S12 as mentioned by Robbie et al.[3] in the above two equations (Equations S6 and S7) to develop the apparent rate constants of DHN photooxidation and juglone formations steps, respectively.

$$\frac{dC_{DHN}}{dt} = -\left[ k_{obs} \frac{k_{TTET}C_{^3m-TcPP}C_{^3O_2}}{k_{IC} + k_{FL} + k_d C_{solvent} + k_{obs}C_{DHN}} \right] C_{DHN} = -k_{app1}C_{DHN} \tag{S13}$$

$$\frac{dC_{Juglone}}{dt} = \left[ k_{obs} \frac{k_{TTET}C_{^3m-TcPP}C_{^3O_2}}{k_{IC} + k_{FL} + k_d C_{solvent} + k_{obs}C_{DHN}} \right] C_{DHN} = k_{app2}C_{DHN} \tag{S14}$$

where the $k_{app1}$ and $k_{app2}$ are the apparent rate constants of DHN photooxidation and juglone formation steps and can be evaluated by fitting experimental data.

**Intermediate rate constants evaluation of DHN photooxidation**

DHN photooxidation can be elaborated using the subsequent elementary reactions:

$$^1\text{m-TcPP} \xrightarrow{\quad k_{hv} \quad} {}^1\text{m-TcPP*}$$

$$^1\text{m-TcPP*} \xrightarrow{\quad k_{ISC} \quad} {}^3\text{m-TcPP}$$

$$^3\text{m-TcPP} + {}^3\text{O}_2 \xrightarrow{\quad k_{TTET} \quad} {}^1\text{m-TcPP} + {}^1\text{O}_2$$

$$\text{DHN} + {}^1\text{O}_2 \xrightarrow{\quad k_{obs} \quad} \text{Juglone}$$
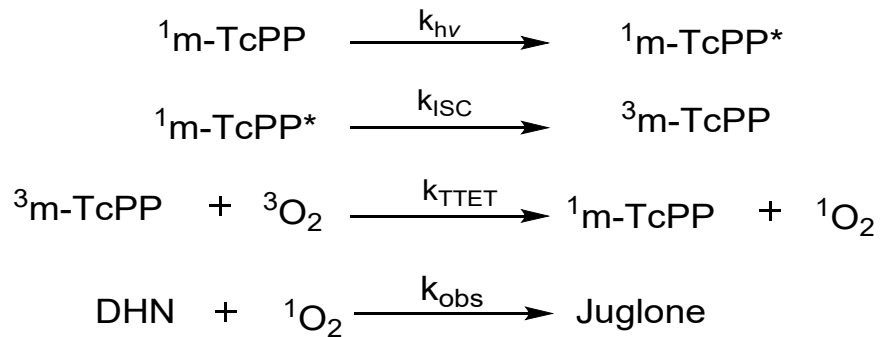
We employed gaussian 09 software package with the B3LYP density functional theory (DFT) method with a basis set of 6-31g(d,p) to determine the frequency, geometry optimization and transition states of these reactions. The transition state was confirmed with at least one imaginary frequency while the ground and excited states simulations were confirmed by stationary point. Transition state theory is typically used to evaluate rate constant of a chemical reaction, which is based on the subsequent quantum mechanical formalism[4].

$$k^{TST} = \sigma\kappa\frac{k_B T}{h}\left(\frac{RT}{P_0}\right)^{\nabla n} e^{-\Delta G^{0,\neq}/RT} \qquad (S15)$$

$$\Delta G^{0,\neq} = G_{TS}^0(T) - G_{\text{Reactant}}^0(T) \qquad (S16)$$

where the parameters $k_B$, h and R represent the Boltzmann, Planks and universal gas constants with values of 1.38E-23J K$^{-1}$, 6.626E-34J s$^{-1}$ and 8.314J mol$^{-1}$ K$^{-1}$, respectively. T, Po and $\Delta G^{0,\neq}$ are the temperature, pressure and Gibbs free energy difference between transition and reactants. The parameter σ indicates reaction path degeneracy (its value for C1 is 1[5]), n indicates molecular reaction (Δn=n-1), and $\kappa$ is transmission of tunneling effect and evaluated using Bell correlation [6], which is presented below:
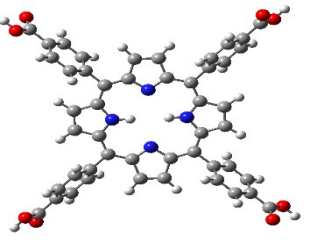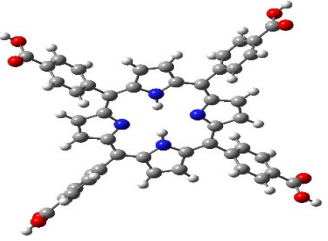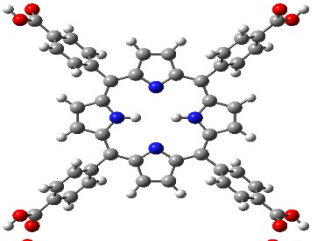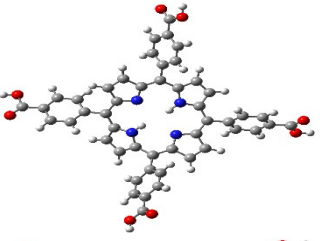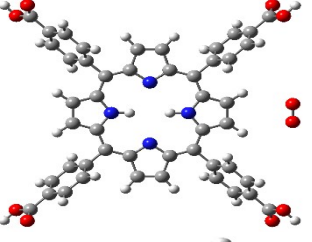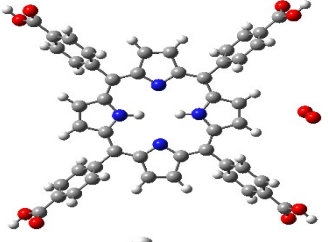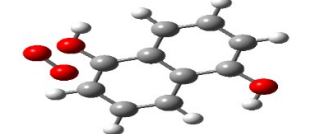
$$\kappa = \kappa_{BELL} = \frac{u}{2}\sin\left(\frac{u}{2}\right) - \sum_{n=1}^{\infty}(-1)^n \frac{\exp\left(\frac{u-2n\pi}{u}\right)\left(\frac{V_0}{k_B T}\right)}{\frac{u-2n\pi}{u}} \qquad (S17)$$

$$u = \frac{h\nu^*}{k_B T} \qquad (S18)$$

where the parameter $V_o$ indicates the barrier height, and $\nu^*$ shows the imaginary frequency of the transition state. We solved these equations for each reaction step and evaluated their corresponding rate constants. These rate constants are intrinsic rate constants which depend on the intrinsic properties such as the optimized geometry, frequency and Gibbs free energy of the molecules rather than their transport properties. Because of this fact, these rate constants were not considered in the kinetics comparison of homogeneous and heterogeneous photocatalysis in photomicroreactors. Table S1 summarizes the optimized structures of reactants and transition states, imaginary frequency, Gibbs free energy and intrinsic rate constants of the above DHN photooxidation reaction steps. It can be seen that the intrinsic rate constant of ISC step ($k_{ISC}$) was

greater than the other intermediate rate constants because of high transition state imaginary frequency and low energy barrier between the reactant ($^1$m-TcPP$^*$) and transition state of this step.

**Table S1** Optimized structure of reactant and transition states, imaginary frequency, Gibbs free energy and intrinsic rate constants of DHN photooxidation reaction steps

| Rxn steps | Reactant | Transition state | Imaginary frequency (cm$^{-1}$) | $\Delta G^{0,\neq}$ (kJ/mol) | $k^{TST}$ (s$^{-1}$) |
|---|---|---|---|---|---|
| 1 |  |  | 26.92 | 4.67 | $k_{h\nu}$=9.579E+11 |
| 2 |  |  | 55.09 | 3.78 | $k_{ISC}$=1.376E+12 |
| 3 |  |  | 18.06 | 22.21 | $k_{TTET}$=2.114E+10 |
| 4 |  |  | 33.97 | 16.90 | $k_{obs}$=1.782E+11 |

**Shelden E-factors evaluation**

We evaluated Sheldon E-factor for both the homogeneous and heterogeneous photocatalysis in photomicroreactors as follows:

Heterogeneous photocatalysis in the photomicroreactor

Weight of DHN = 0.012013g

Weight of juglone= 0.01034 g

Weight of Oxygen = 0.0785 g

Weight of Solvent =0.82425 g

E1= ((0.012013)-0.01034)/0.01034= 0.162

E2= ((0.012013+0.0785)-0.01034)/0.01034=7.75

E3= ((0.012013+0.82425)-0.01034)/0.01034=79.88

E3= ((0.012013+0.82425+0.0785)-0.01034)/0.01034=87.5

**Temperature logging inside irradiation compartment of HLPMR**

To determine the efficiency of the cooling system (three integrated fans) in place of HLPMR, we performed temperature logging of the juglone synthesis process for both homogeneous and heterogeneous photocatalysis under experimental operating conditions. We installed two temperature sensors at the inside and outside of the irradiation compartment of this HLPMR for temperature measurement and consistently logged temperature for one-hour operation with five-minute intervals. The scalability of homogeneous photocatalysis was optimized under high irradiation power (P=600 W) while the best conditions for the scalability of heterogeneous photocatalysis were found at low irradiation power (P=360 W). Thus, we used these irradiation powers for the temperature logging of the DHN photooxidation process using both homogeneous and heterogeneous photocatalysis, as presented in Fig. S2.

Overall, the rise in inside temperature from outside side temperature in the case of homogeneous photomicroreactor was 12$^{\circ}$C while this temperature increase in heterogeneous

photocatalysis was found to be 5 °C. Moreover, the maximum inside temperature was escalated to 38 °C and 30.9 °C for both homogeneous and heterogeneous photocatalysis. Such an increase in temperature is quite normal in air-cooled LEDs, stemming from the low heat capacity of air under this forced convection cooling system. In contrast, water-cooled LEDs are waterproof in nature, and temperature is efficiently maintained to room temperature in these LEDs by circulating small water flow due to its large heat capacity. However, waterproof LEDs are more expensive than airproof LEDs and cannot be used in this HLPMR. Secondly, the reaction kinetics of photon-driven transformations mainly rely on the photon absorbance of the reaction medium, and typically correlations are developed between apparent rate constants and photon flux for these processes [7, 8]. Based on this fact, the effect of temperature on the photochemical transformation performance (i.e. product yield, selectivity, and so on) is typically not taken into consideration in these investigations.
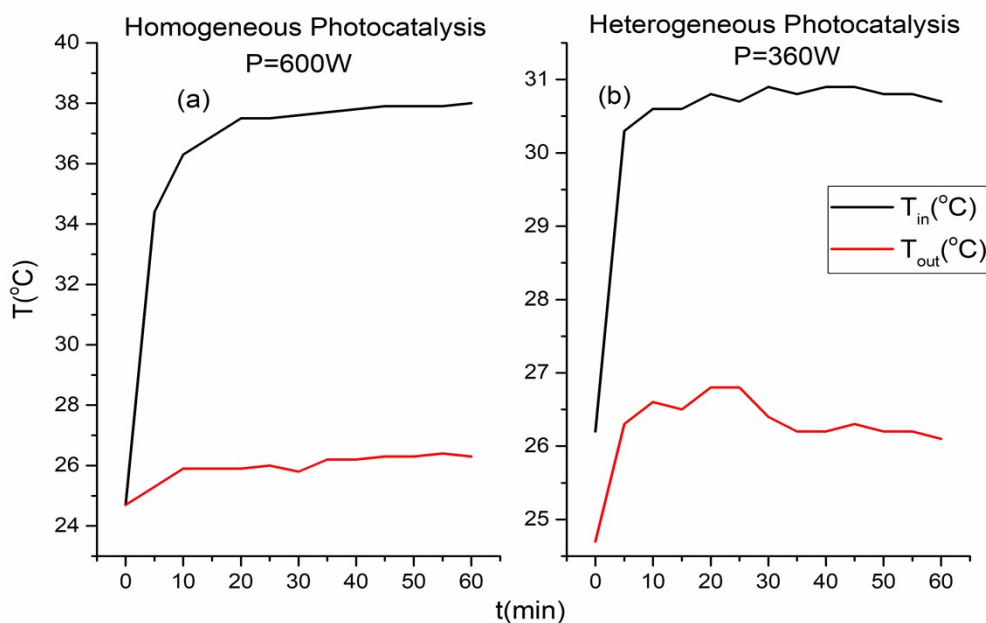


**Fig.S2** Temperature logging for consistently one-hour DHN photooxidation process (a) homogeneous photocatalysis ($Q_L$=5.0 ml/min, $Q_G$=100 ml/min, $C_{DHN}$=0.1M) (b) heterogeneous photocatalysis ($Q_L$=1.5 ml/min, $Q_G$=60 ml/min, $C_{DHN}$=0.05 M)

To further examine the performance of these cooling fans under the worst-case scenario, we operated this photomicroreactor only under solvent flow without employing any photocatalyst for both homogeneous and heterogeneous processes. Fig. S3 shows the inside temperature of the irradiation compartment for both homogeneous and heterogeneous

photocatalysis with and without employing the photocatalyst. The average rise in temperature without using m-TcPP (homogeneous catalysts) in homogeneous photocatalysis was found to be 4.7 °C whereas this temperature rise was 14.5 °C using deactivated photocatalyst (Amb-m-TcPP (DeA)) instead of employing activated photocatalyst (Amb-m-TcPP (A)) for heterogeneous photocatalysis. It shows the outstanding ability of both homogeneous and heterogeneous photocatalysts to absorb visible light photons and drop inside temperature of the irradiation compartment of HLPMR. Furthermore, the maximum temperature was 43.8 ° C and 45.6 ° C without using photocatalysts for homogeneous and heterogeneous processes, which are still under controllable limits. Thus, photocatalysts and cooling fans in HLPMR are quite enough to operate HLPMR under the controllable operating limit and efficiently dissipate heat to avoid any possibility of initiating thermal explosion, which normally triggers through the over-irradiation of photomicroreactor due to the meager cooling system in place.
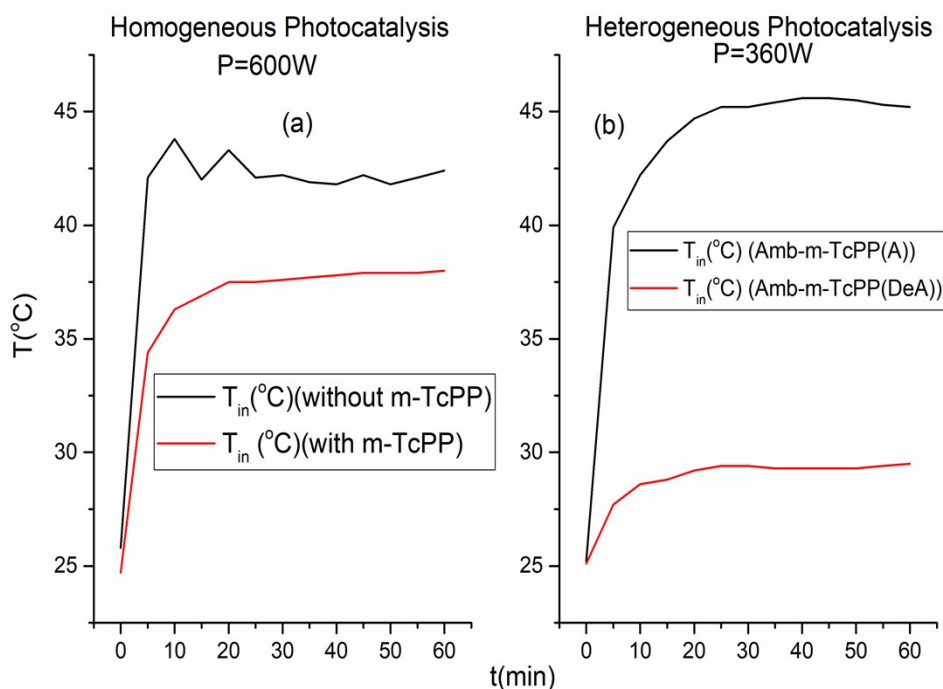


**Fig.S3** Inside temperature of HLPMR irradiation compartment with and without using photocatalysts (a) homogeneous photocatalysis ($Q_L$=5 ml/min) (a) heterogeneous photocatalysis ($Q_L$=1.5 ml/min)

External cooling systems such as portable air-conditioning units can be employed to control the temperature of photochemical processes. We also examined the impact of the external cooling system on the current photomicroreactor by installing a 1-ton portable AC unit,

as indicated in Fig. S4. The temperature logging under this condition can be seen in Fig. S5a. The inside and out temperatures of HLPMR were almost identical and even at some points inside temperature was lower than the outside temperature by employing such an external AC unit. However, juglone yield could not be improved by employing this additional cooling system under similar operating conditions as indicated by Fig. S5b and using this external AC unit reduces the green credentials of this HLPMR according to the green chemistry principle 6 (Energy efficient by design). This temperature logging campaign indicates that the low heat capacity of air is mainly responsible for such temperature rise in HLPMR, but this temperature rise is under controllable range and does not have any influence on the DHN photooxidation performance.
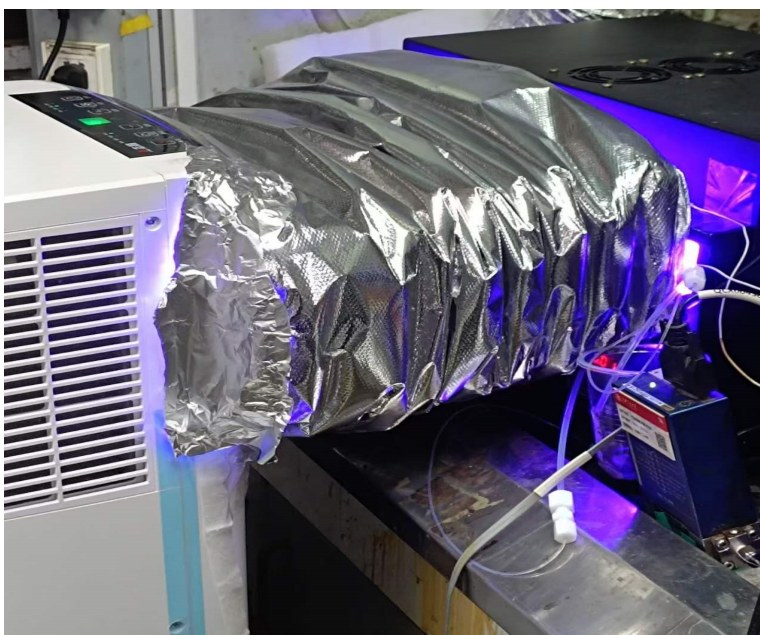


**Fig.S4** Use of 1-ton external AC unit to control the temperature of irradiation compartment of HLPMR
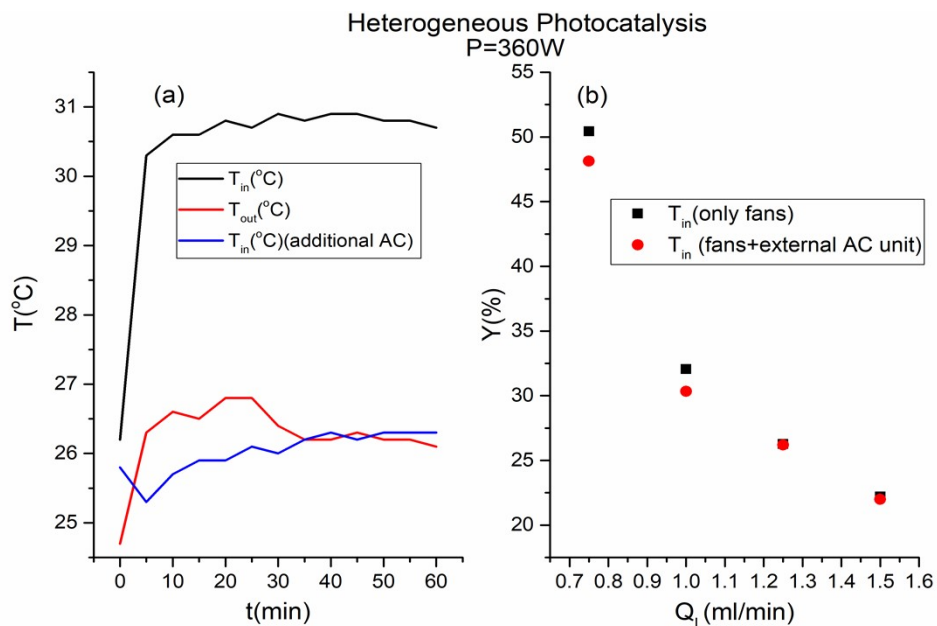
**Fig.S5** Use of additional portable AC unit (a) Temperature logging with additional portable AC unit (b) impact of inside temperature on juglone yield at $Q_L$=0.5-1.25 ml/min, $Q_G$=30-60 ml/min and $C_{DHN}$=0.05 M)

## Experimentation through homogeneous photocatalysis in photomicroreactor
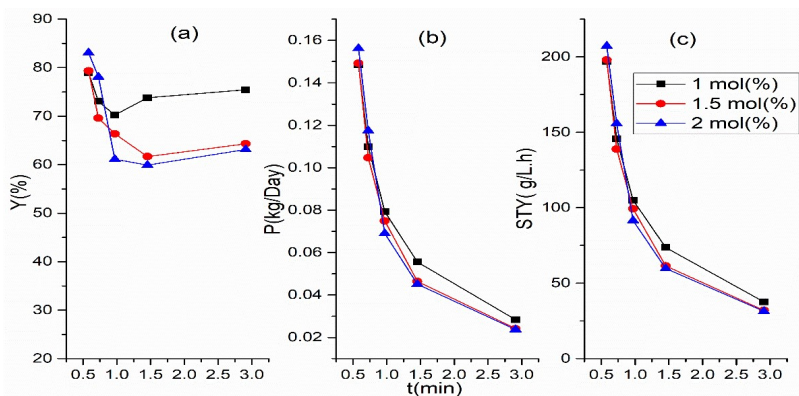


**Fig.S6** Homogeneous DHN photooxidation by varying m-TcPP loading, $Q_L$=1-5 ml/min, $Q_G$=9.8-49 ml/min, $V_1$=31.42 ml, $C_{DHN}$=0.15 M, P=600 W, BPR=75psig and solvent=i-PrOH (a) yield (b) productivity (c) space time yield
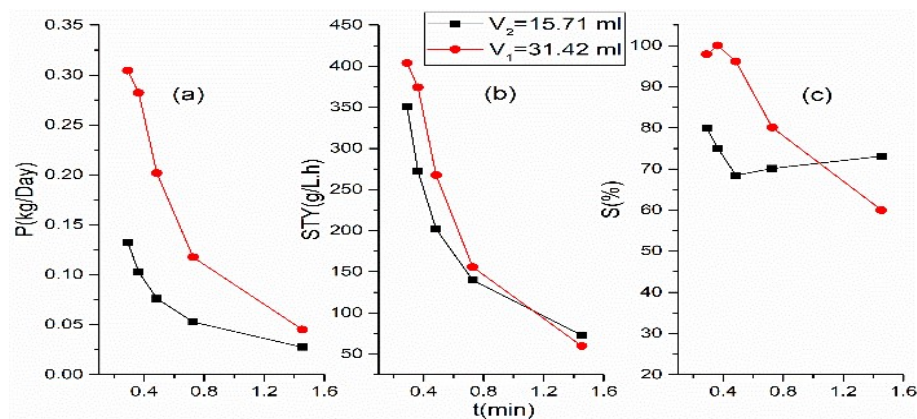
**Fig.S7** Effect of PFA capillary volume on homogeneous photooxidation performance at various residence time (a) productivity (b) space time yield (c) selectivity Reaction conditions: $Q_L$=1-10 ml/min, $Q_G$=9.8-98 ml/min, m-TcPP loading=2 mol%, $C_{DHN}$=0.15 M, P=600 W, the operational pressure was 5.2 bar, and the solvent was i‑PrOH.
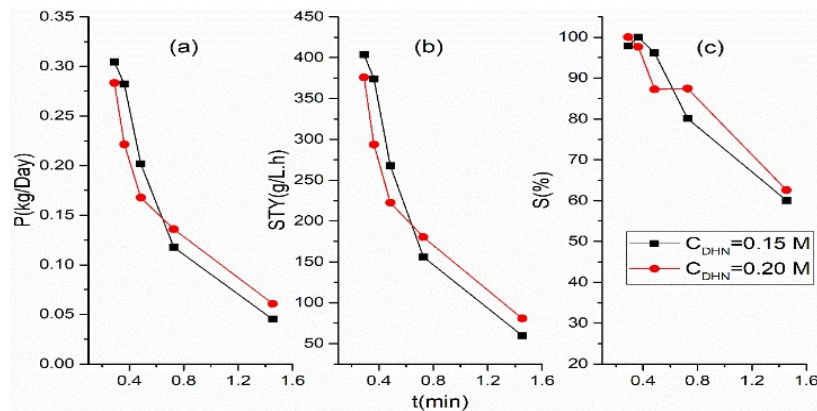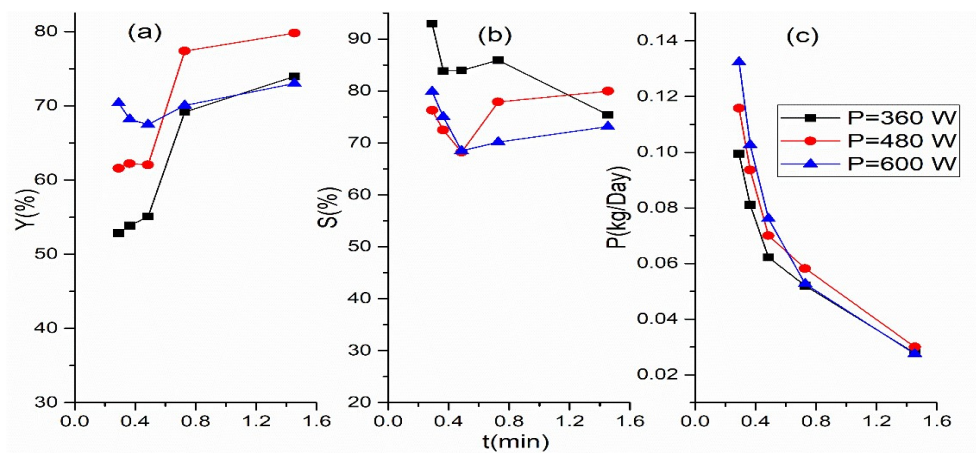


**Fig.S8** Effect of DHN concentration on homogeneous DHN photooxidation performance at various residence time (a) productivity (b) space time yield (c) selectivity Reaction conditions: $Q_L$=2-10 ml/min, $Q_G$=19.6-98 ml/min, m-TcPP loading=2mol%, $V_1$=31.42 ml, P=600 W, the operational pressure was 5.2 bar, and the solvent was i-PrOH.

**Fig.S 9** Effect of LED irradiation power on homogeneous DHN photooxidation at various residence time (a) yield (b) selectivity (c) productivity Reaction conditions: QL=1-5 ml/min, QG=9.8-49 ml/min, m-TcPP loading=2 mol%, V2=15.71 ml, CDHN=0.15 M, the operational pressure was 5.2 bar, and the solvent was *i*-PrOH.
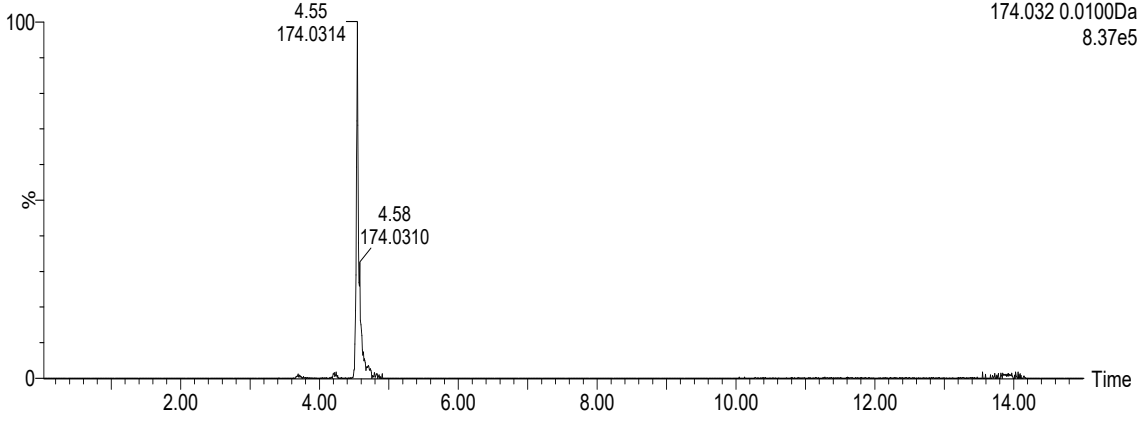
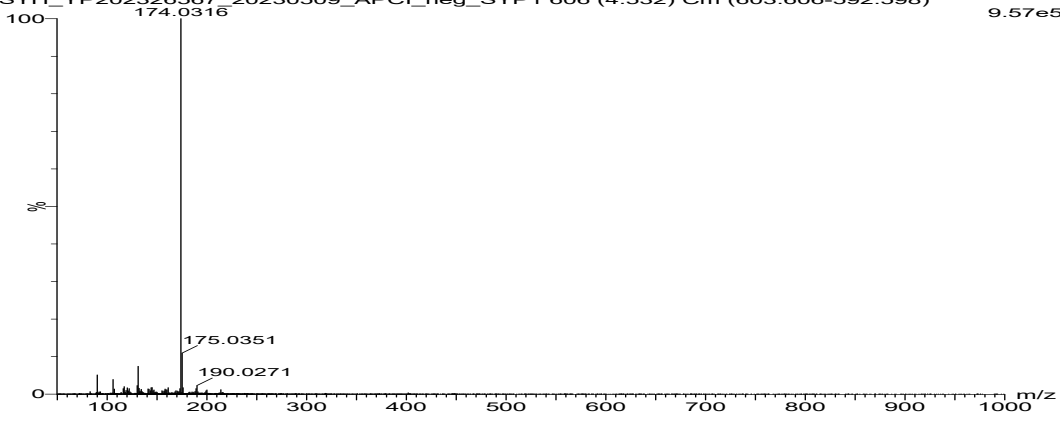## Purified juglone product

# LC-MS of the purified juglone

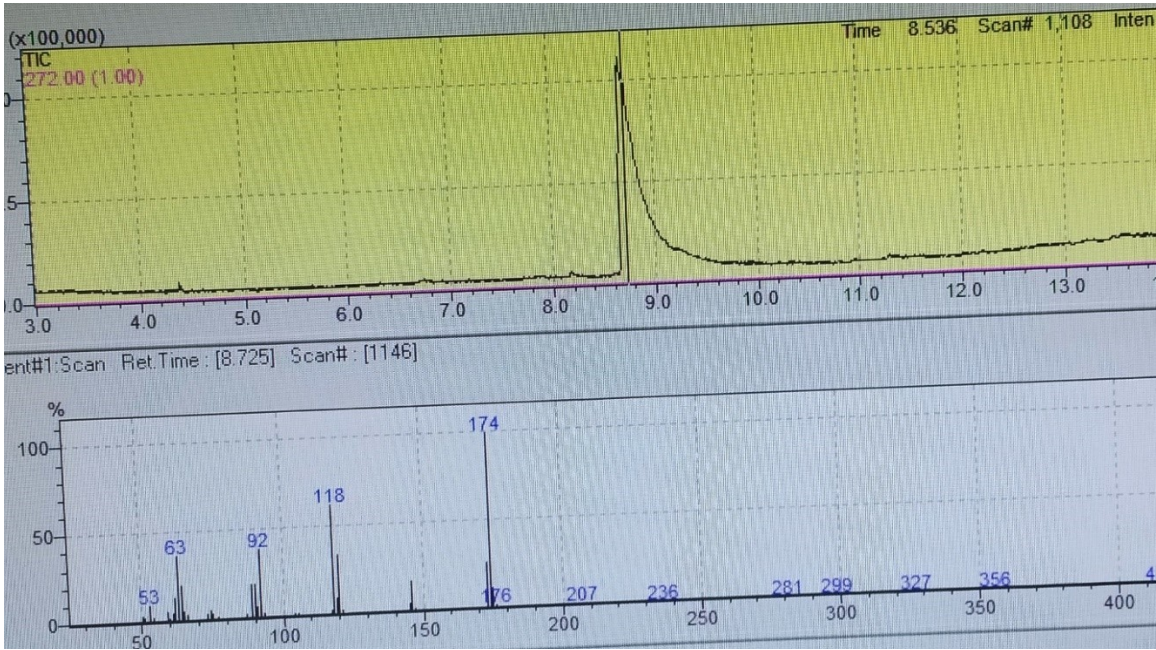SYH_YP202326567_20230509_APCI_neg_SYP1

1: TOF MS AP-
174.032 0.0100Da
8.37e5



SYH_YP202326567_20230509_APCI_neg_SYP1 606 (4.532) Cm (603:606-592:598)          9.57e5



| Mass | Calc. Mass | mDa | PPM | DBE | i-FIT | Norm | Conf(%) | Formula |
|------|-----------|-----|-----|-----|-------|------|---------|---------|
| 174.0316 | 174.0317 | -0.1 | -0.6 | 8.0 | 706.3 | n/a | n/a | C10H6O3 |

**GC-MS of the currently and commercially produced juglone**



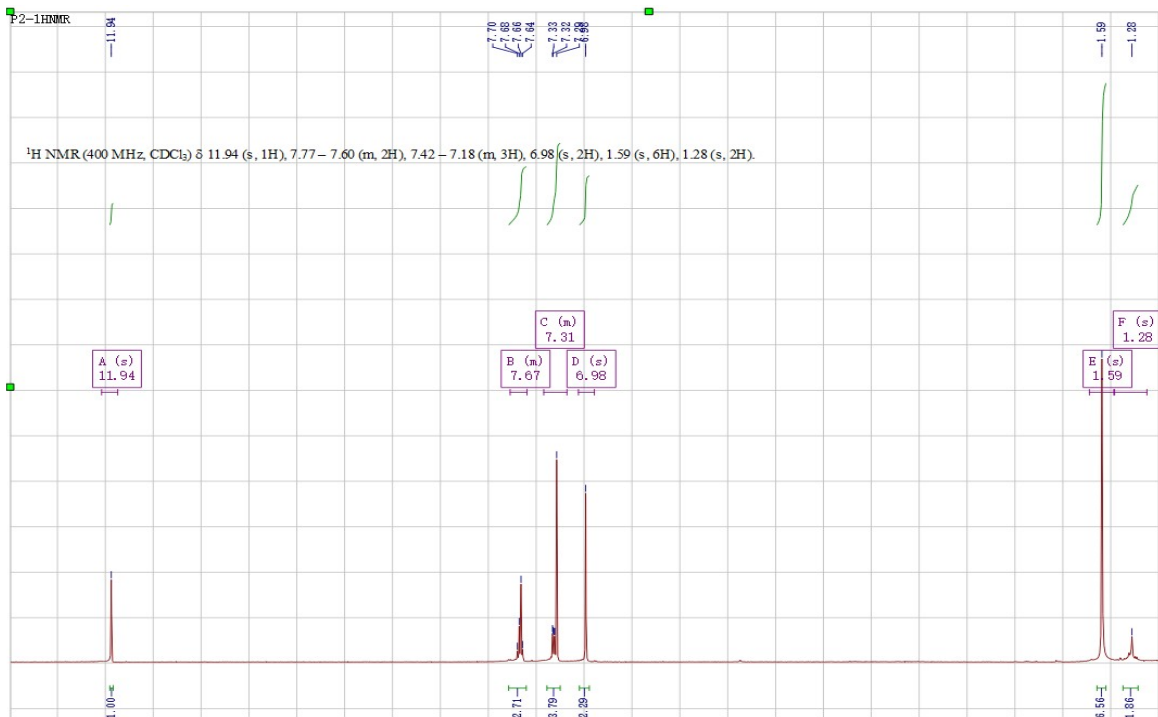GC-MS,m/z:174[M⁺],174,118,92 (currently produced juglone)
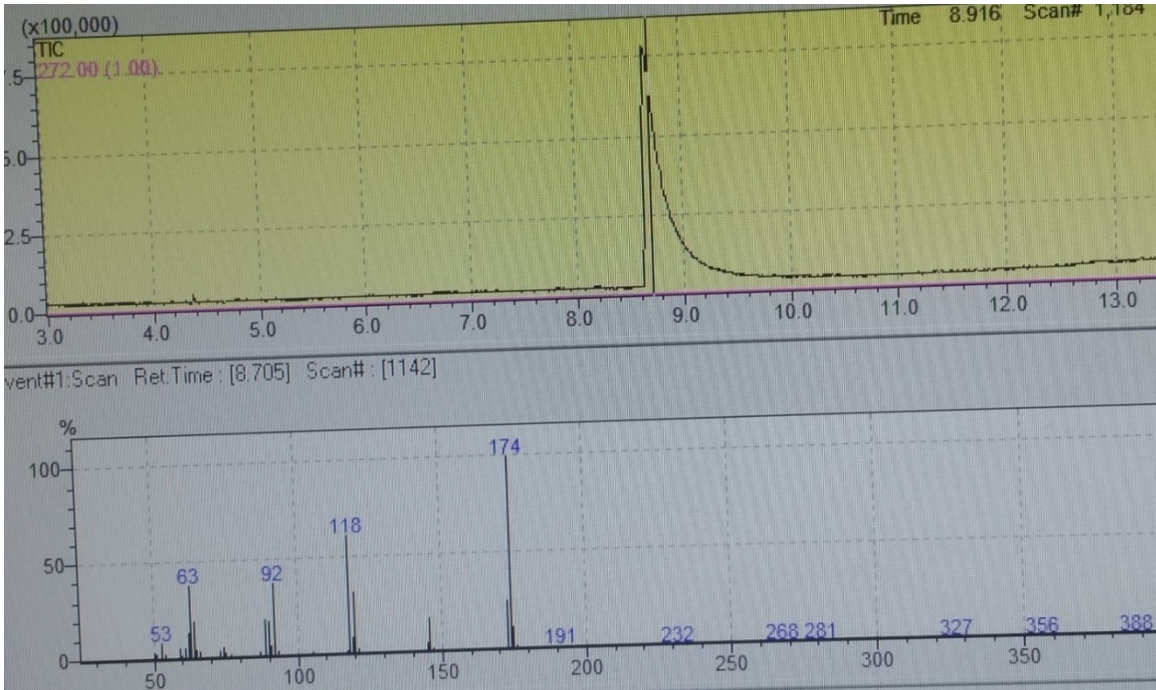


GC-MS,m/z:174[M+],174,118,92 (commercial juglone)

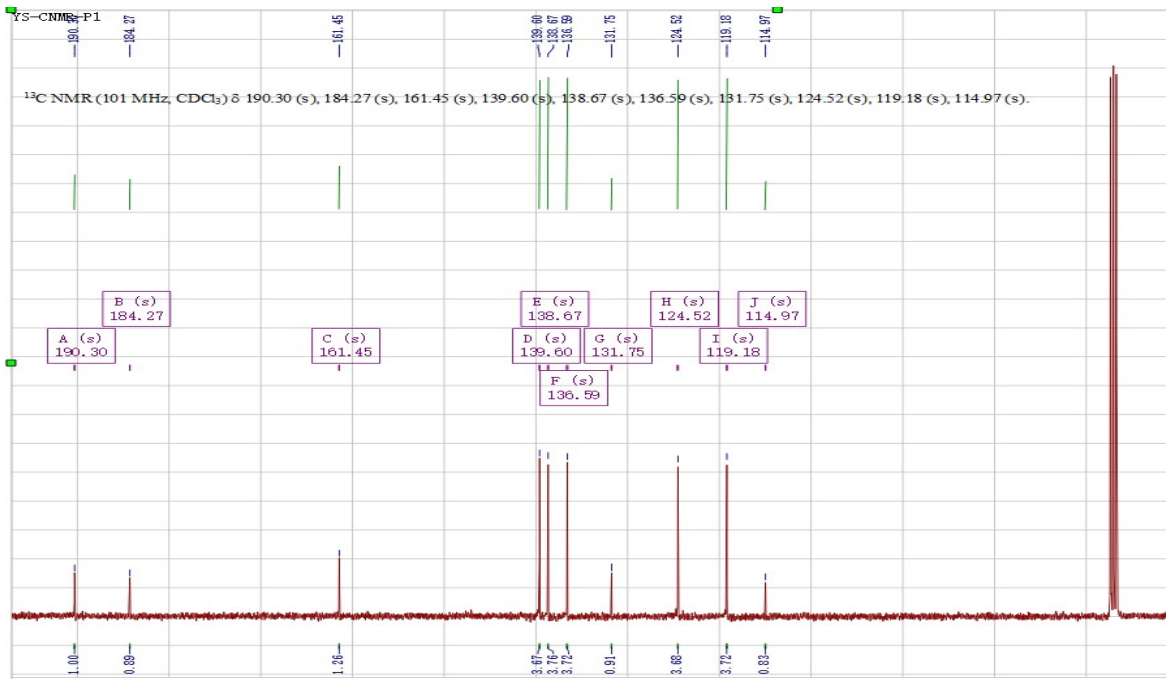**¹H NMR of the currently and commercially produced juglone**
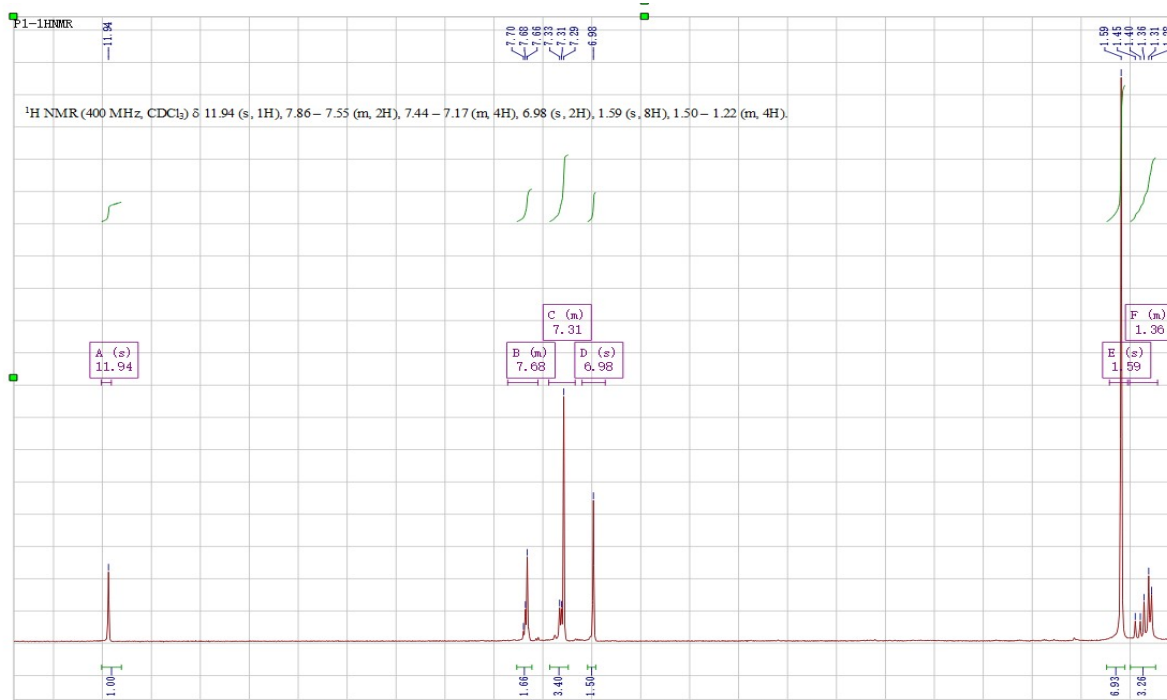


¹H NMR (400 MHz, CDCl₃) δ 11.94 (s, 1H), 7.86 – 7.55 (m, 2H), 7.44 – 7.17 (m, 4H), 6.98 (s, 2H), 1.59 (s, 8H), 1.50 – 1.22 (m, 4H). (currently produced juglone)
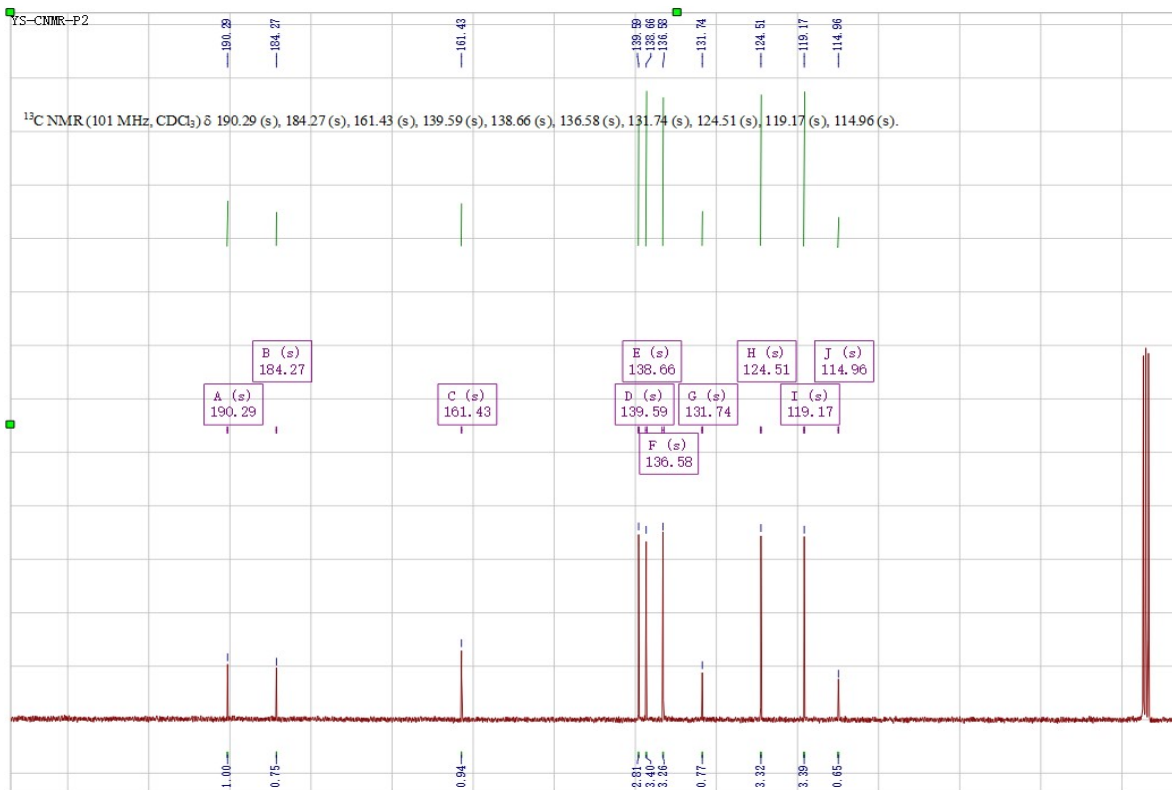


¹H NMR (400 MHz, CDCl3) δ 11.94 (s, 1H), 7.77 – 7.60 (m, 2H), 7.42 – 7.18 (m, 3H), 6.98 (s, 2H), 1.59 (s, 6H), 1.28 (s, 2H). (commercial juglone)

## ¹³C NMR of the currently and commercially produced juglone



¹³C NMR (101 MHz, CDCl₃) δ 190.30 (s), 184.27 (s), 161.45 (s), 139.60 (s), 138.67 (s), 136.59 (s), 131.75 (s), 124.52 (s), 119.18 (s), 114.97 (s). (currently produced juglone)

$^{13}$C NMR (101 MHz, CDCl3) δ 190.29 (s), 184.27 (s), 161.43 (s), 139.59 (s), 138.66 (s), 136.58 (s), 131.74 (s), 124.51 (s), 119.17 (s), 114.96 (s). (commercial juglone)

## HPLC analysis method and calibration

| | |
|---|---|
| Machine | Shimadzu LC, 16 Japan |
| Column Details | shim-pack column (GWS C18, 5 μm, 4.6 × 250 mm) |
| Eluent | 0.1 M Acetic acid in water / methanol (50/50) (v/v) % |
| Flow rate | 0.8 ml/min |
| Temperature | 40 °C |
| Injection volume | 1 μL |
| UV detection | 230 nm (DHN) and 242 nm (Juglone) |
| Retention time | 10.17 min (DHN) and 20.58 min (Juglone) |
| Method runtime | 35 min |



DHN Calibration
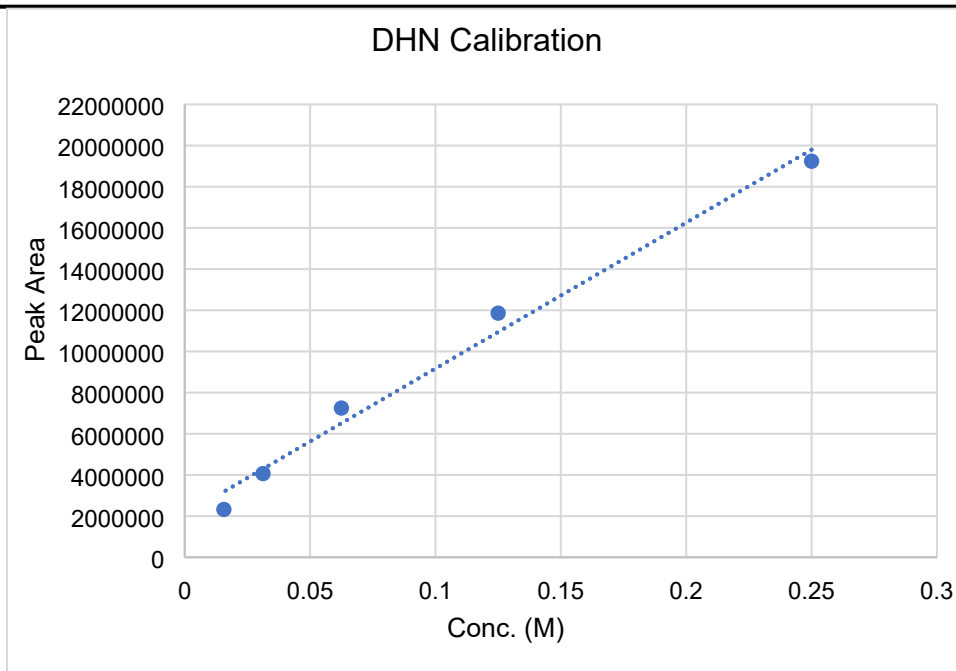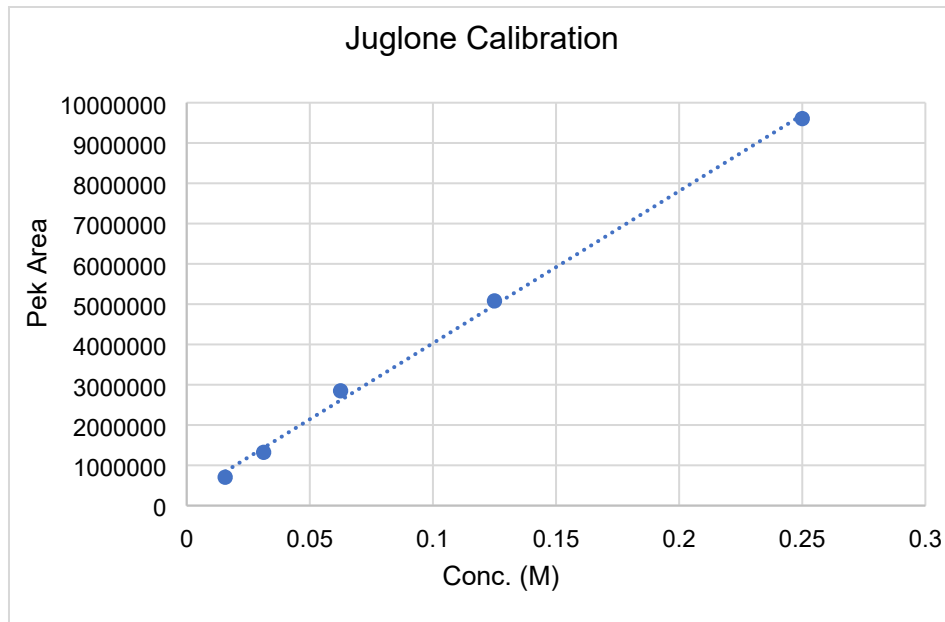
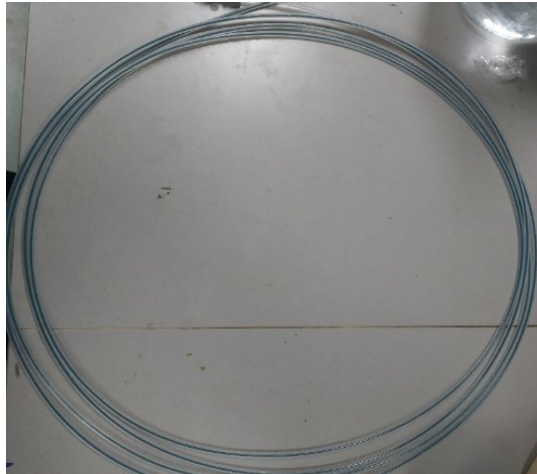**Adsorption and desorption isotherms for BET surface area**
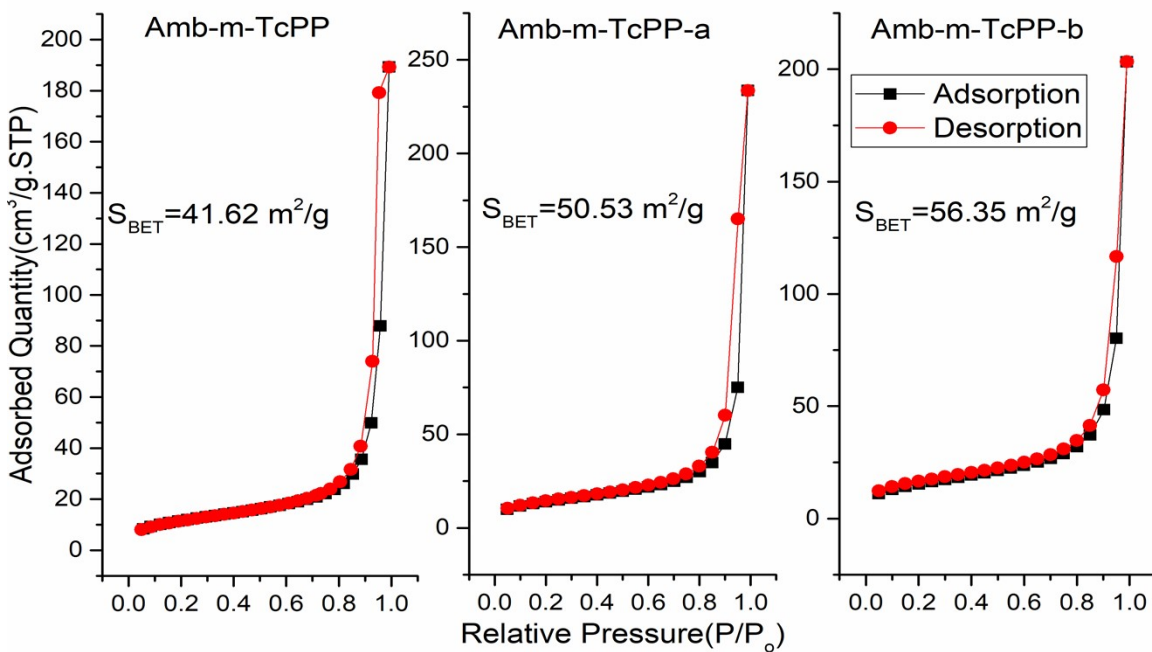
**PFA microchannel containing Amb-m-TcPP**

PMR1(7.85 ml)

PMR2(15.7ml)

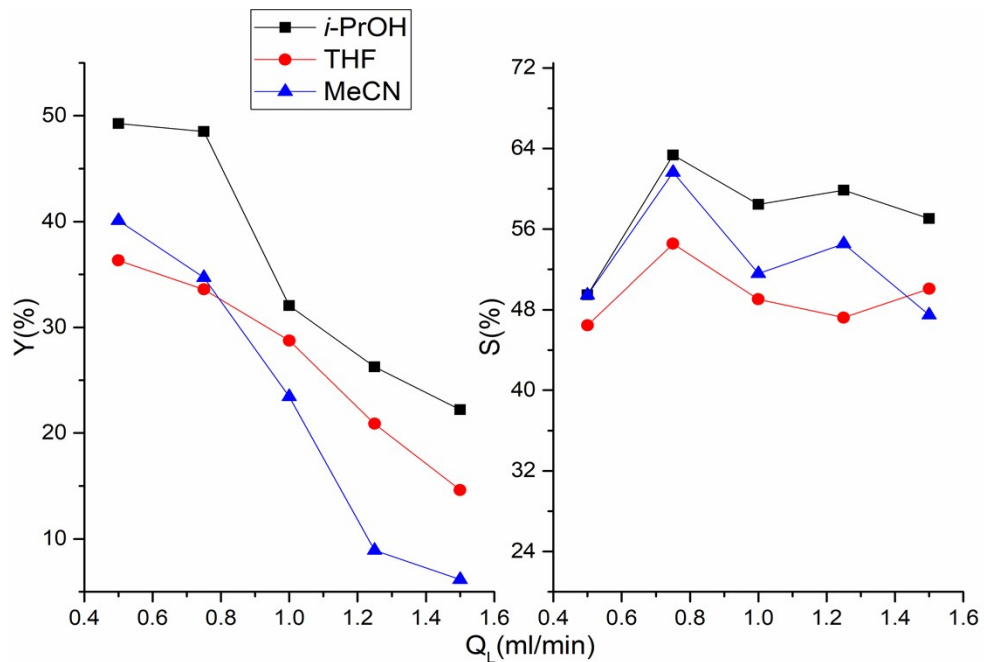**Heterogeneous DHN photooxidation under various solvents**



**Fig.S10** Influence of using various solvents on DHN photooxidation performance using PMR. Conditions: $Q_L$=0.5-1.5 ml/min, $Q_G$=30-60 ml/min, $\tau_{PMR1}$=3.18-9.55 min, Amb-m-TcPP, P=360 W and $C_{DHN}$ =0.05 M

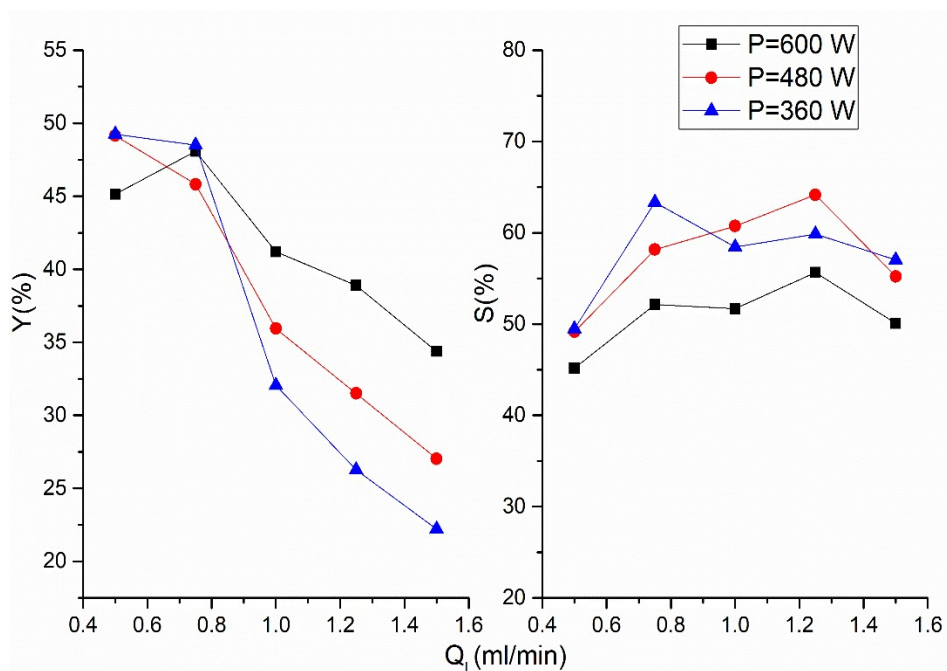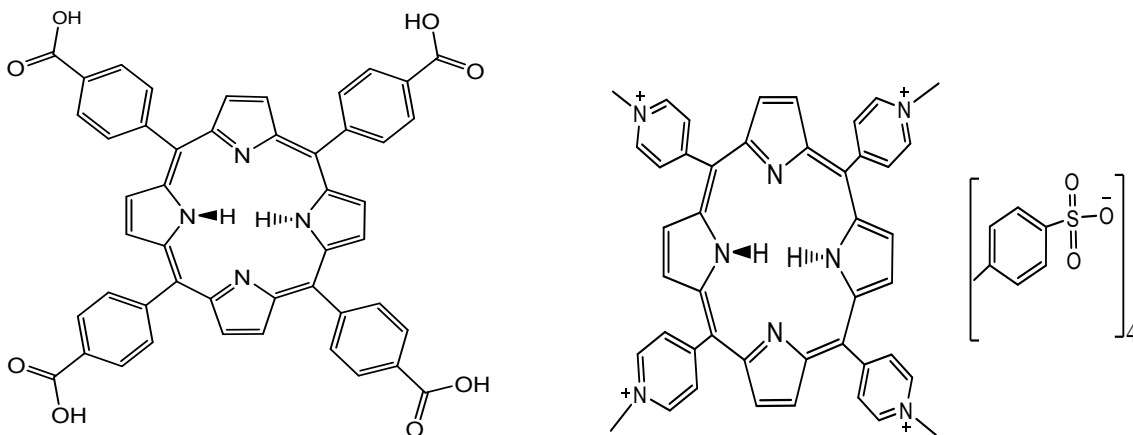**Heterogeneous DHN photooxidation under various LED power**

**Fig.S11** Influence of various LED power in DHN photooxidation performance Conditions: $Q_L$=0.5-1.5 ml/min, $Q_G$=30-60 ml/min, $\tau_{PMR1}$=3.18-9.55 min, Amb-m-TcPP, solvent=i-PrOH and $C_{DHN}$ =0.05 M

## Structures of m-TcPP and TMPyP



meso-tetracarboxyphenylporphyrine (m-TcPP)

Tetrakis(1-methyl-4-pyridinio) porphyrin tetra(p-toluenesulfonate)

## Surface morphology of SiO$_2$-m-TcPP and SiO$_2$-TMPyP

SEM images of SiO$_2$-m-TcPP are presented in Fig.S12 a-c, while these images for SiO$_2$-TMPyP are spotlighted in Fig.S12 d-f. There is layer of m-TcPP and TMPyP developed over SiO$_2$ particles in both photocatalysts, however there are some surface inhomogeneities on certain locations. Furthermore, SiO$_2$-m-TcPP and SiO$_2$-TMPyP particle sizes are smaller, non-uniform in shape and have sharper edges compared to Amb-m-TcPP, which possibly give rise to high scattering of incident light. Fig.S13 a and b show EDS mapping of SiO$_2$-m-TcPP and SiO$_2$-TMPyP, and the carbon contents in these two photocatalysts are much lower than those of Amb-m-TcPP, indicating weakly developed layer of m-TcPP and TMPyP over SiO$_2$ particles.
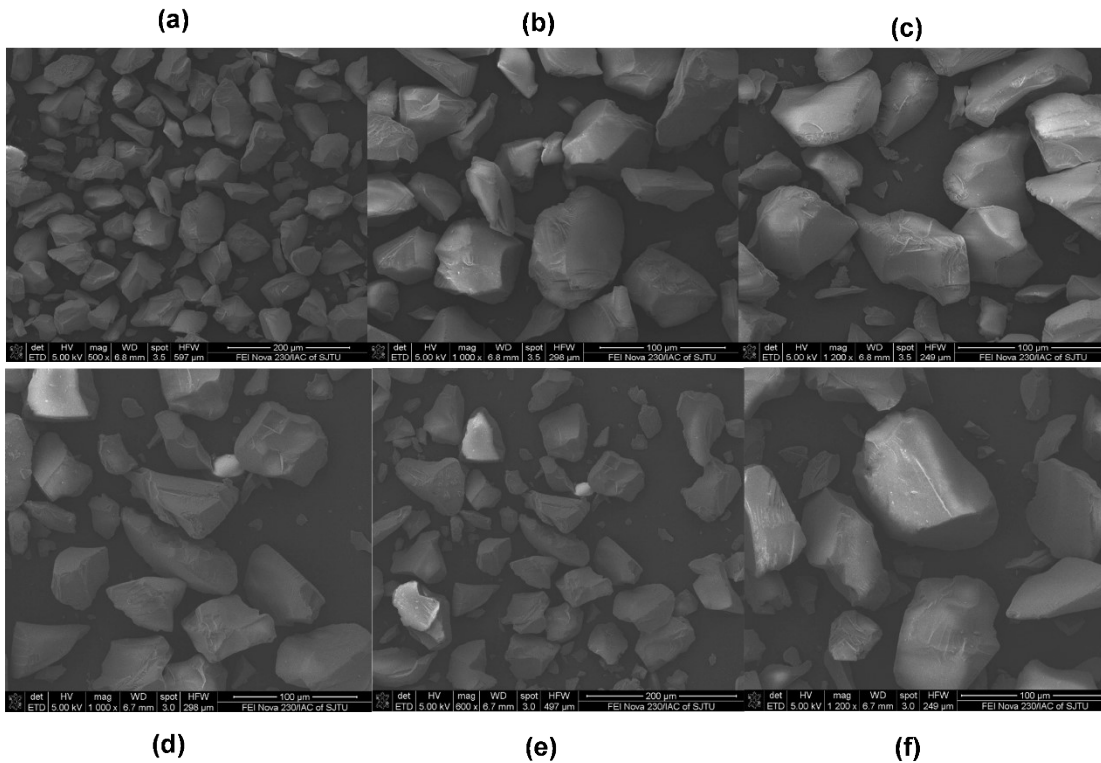
**Fig.S12** SEM images of photocatalysts (a)-(c) SiO$_2$-m-TcPP (d)-(f) SiO$_2$-TMPyP



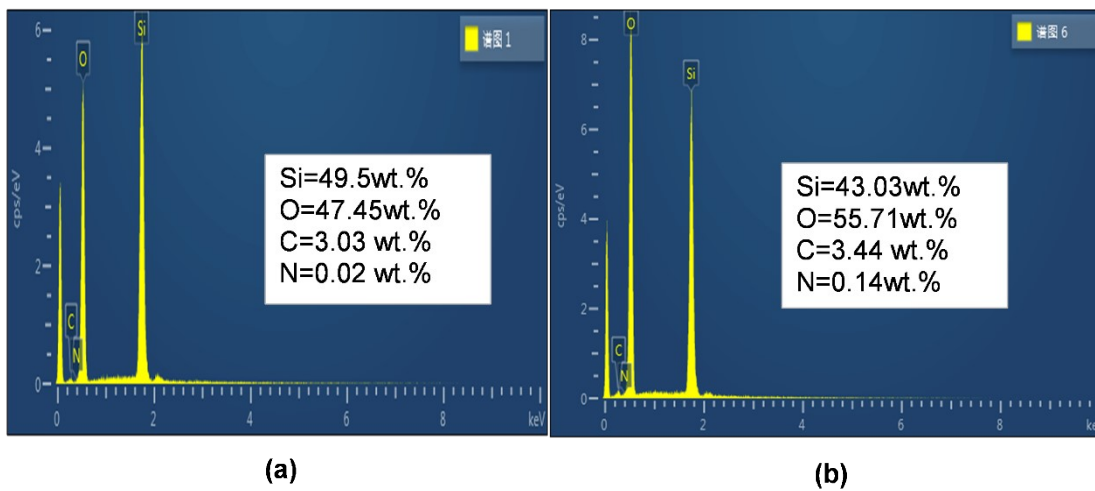| (a) | (b) |
|-----|-----|
| Si=49.5wt.% | Si=43.03wt.% |
| O=47.45wt.% | O=55.71wt.% |
| C=3.03 wt.% | C=3.44 wt.% |
| N=0.02 wt.% | N=0.14wt.% |

**Fig.S13** EDS mapping of photocatalysts (a)SiO$_2$-m-TcPP (b)SiO$_2$-TMPyP

## References

1. S.-y. Takizawa, R. Aboshi and S. Murata, *Photochemical & Photobiological Sciences*, 2011, **10**, 895-903.

2.      A. Beltrán, M. Mikhailov, M. N. Sokolov, V. Pérez-Laguna, A. Rezusta, M. J. Revillo and F. Galindo, *Journal of Materials Chemistry B*, 2016, **4**, 5975-5979.

3.      R. Radjagobalou, J.-F. Blanco, O. Dechy-Cabaret, M. Oelgemöller and K. Loubière, *Chemical Engineering and Processing - Process Intensification*, 2018, **130**, 214-228.

4.      E. Dzib, J. L. Cabellos, F. Ortíz-Chi, S. Pan, A. Galano and G. Merino, *International Journal of Quantum Chemistry*, 2019, **119**, e25686.

5.      M. Spiegel, *Journal of Chemical Information and Modeling*, 2022, **62**, 2639-2658.

6.      C. Doubleday, R. Armas, D. Walker, C. V. Cosgriff and E. M. Greer, *Angewandte Chemie International Edition*, 2017, **56**, 13099-13102.

7.      L. Buglioni, F. Raymenants, A. Slattery, S. D. A. Zondag and T. Noël, *Chemical Reviews*, 2022, **122**, 2752-2906.

8.      M. Pasha, S. Liu, M. Shang, M. Qiu and Y. Su, *Chemical Engineering Journal*, 2022, **445**, 136663.